NJC

PAPER

View Article Online
View Journal

Cite this: DOI: 10.1039/c5nj03099d

ZnO decorated with organic nanoparticles based sensor for the ratiometric selective determination of mercury ions†

Narinder Kaur,‡[a] Jasminder Singh,‡[b] Pushap Raj,[b] Narinder Singh,*[b] Harpreet Singh,[c] Sanjeev K. Sharma,*[a] Deuk Young Kim[a] and Navneet Kaur*[de]

Received (in Montpellier, France) 5th November 2015,
Accepted 22nd November 2015

DOI: 10.1039/c5nj03099d

www.rsc.org/njc

ZnO nanoparticles decorated with organic receptor 1 (**R1**) have been prepared and the resultant compound (**N1**) was investigated for its metal recognition ability. **N1** was found to be selective for mercury ions (Hg^{2+}) in a DMSO/water mixture in a ratio of 7 : 3 and possessed no interference from any of the potential interferent metal ions. The crystal size and morphology of ZnO is characterized using various spectroscopic and diffraction techniques like scanning electron microscopy, X-ray diffraction (XRD), dynamic light scattering (DLS), *etc.* Surface decoration of the ZnO with receptor 1 is confirmed using NMR spectroscopy. On successive additions of Hg^{2+} ions, the fluoresence intensity of the compound was quenched at 427 nm with enhancement of the peak at 482 nm, which led to ratiometric sensor development for the recognition of mercury ions having a detection limit of 0.19 nM. The prepared receptor was also tested for real sample application by preparing a known concentration of Hg^{2+} solution and it was found to respond well with an accuracy more than 90%.

Introduction

The selective recognition of cations in aqueous or non-aqueous systems is an extremely vital issue, because their excess in the environment has become the reason for various health implications like damage to the central nervous system, diseases of the immune and reproductive systems *etc.*[1–5] Leaching of these heavy metal ions into ground water resources, leading to water contamination, has led to a severe health crisis in many countries, especially in developing countries.[6,7] Among the various cations, the most abundant form of mercury ions, the mercuric ion (Hg^{2+}), is highly poisonous, carcinogenic and has acute cellular toxicity. Due to these reasons mercuric ions are considered to be the worst pollutant among all the metal ions.[8–10] The extremely toxic nature of mercury in the earth's crust and to human beings came into the limelight after the Minamata incident in Japan in 1965.[11,12] The severe toxicity of mercury ions can be attributed to their easy invasion of the human body through the skin, respiratory system, cell membranes and gastrointestinal tissues, causing neurological disorders such as acrodynia, Hunter–Russell syndrome and Minamata disease.[13,14] Naturally occurring methyl mercury (formed by the biomethylation of mercuric ions in aquatic systems) *i.e.* the organic form of mercury has been deemed responsible for causing various neurological disorders. This methyl mercury accumulates in the food chain and can easily cross the blood–brain barrier after human ingestion, leading to its fatal effects on human health.[15–17] However, inorganic mercury ions (Hg^{2+}) are more nephrotoxic than the organic form ($MeHg^{+}$) because they accumulate in kidney proximal tubule cells.[18] Therefore, the detection of mercury ions is of paramount importance and could assist in the prevention of harmful effects on the human race from mercury ions. The U.S. environmental protection agency (EPA) has set a maximum of ~2 ppb as its bench mark for food and beverage articles. Thus, the need for a sensor with a detection limit for mercury ions lower than this permissible limit is of great prominence.[19,20]

In the past few years, mercury ions have been detected using various analytical and spectroscopic techniques like atomic absorption spectroscopy (AAS),[21–23] fluorescence spectroscopy,[26,27] inductively coupled plasma spectroscopy[24,25] and electrochemical methods,[28,29] due to their good selectivity, high sensitivity, and

[a] Semiconductor Materials and Device Laboratory, Department of Semiconductor Science, Dongguk University-Seoul, Seoul 100715, Republic of Korea
[b] Department of Chemistry, Indian Institute of Technology (IIT) Ropar, Rupnagar, Punjab 140001, India. E-mail: nsingh@iitrpr.ac.in
[c] School of Mechanical, Materials & Energy Engineering, IIT Ropar, Rupnagar, Punjab 140001, India
[d] Centre for Nanoscience and Nanotechnology (UIEAST), Panjab University, Chandigarh, 160014, India
[e] Department of Chemistry, Panjab University, Chandigarh, 160014, India. E-mail: navneetkaur@pu.ac.in

† Electronic supplementary information (ESI) available. See DOI: 10.1039/c5nj03099d

‡ Both authors contributed equally.

fast analysis. However, these methods require expert handling, laborious sample preparation and cost a fortune. Thus, fluorescent chemosensors have evolved as a suitable alternative and have received more attention for the determination of mercury ions in various samples of environmental and ecological origin. Furthermore, the research field has been paying enormous attention to the development of new fluorescent molecules and, particularly, ZnO based chemosensors are emerging as a new fascinating field due to their excellent optical and electronic properties such as high exciton binding energy (60 meV) and wide energy gap (3.37 eV).[30–35] Moreover, the previous literature has demonstrated the gas sensing performance of ZnO owing to its quantum size effects and various morphologies.[36–38] Nevertheless, only a few reports of decorated ZnO receptors are available for cation detection.[38–40] Lately, the nanomolar (0.4 nM) detection of Co^{2+} by the decoration of imine linked receptors on ZnO has been reported.[41] The imine-linked dipodal Zn^{2+} complex was synthesized and demonstrated for the recognition of multiple cations (Fe^{2+}, Co^{2+} and Cu^{2+}) with a detection range of 100, 500 and 200 nM, respectively.[34] The chromogenic detection of Mg^{2+} and the fluorescence detection of Cr^{3+} were confirmed with benzimidazole based imine linked chemosensors having a detection limit of 79.4–340 μM.[42] Therefore, the available reports on ZnO based receptors for different cation recognition can help us in achieving the desired detection limit and selectivity for the highly toxic mercury ions.

In this paper, we have surface decorated ZnO nanoparticles using **R1**, and the resultant compound (**N1**) was tested for its metal binding abilities and was able to detect Hg^{2+} ions in the nanomolar range. **N1** was also tested for real sample analysis of a Hg^{2+} solution and had an accuracy more than 90%.

Results and discussion

Synthesis of receptor 1 (R1) and its decoration on the surface of ZnO to form N1

The proposed receptor (**R1**) was prepared using a single step condensation reaction between imine linkages containing 2-(2-aminophenyl)benzmidazole and salicylaldehyde in dry methanol. Stirring at room temperature for 3 h, yielded a yellow product, which was filtered and washed using methanol (Scheme 1).

R1 thus formed, was fully characterized using IR, ^{1}H NMR, and ^{13}C NMR (ESI,† S1 & S2). The imine linked (–CH═N) stretching frequency band was observed at 1621 cm^{-1} in the IR spectrum of the receptor (**R1**). Peaks for the imine linkage (–CH═N) at δ 7.27 and at δ 165.9 in the ^{1}H NMR and ^{13}C NMR confirmed the formation of the receptor. For the surface

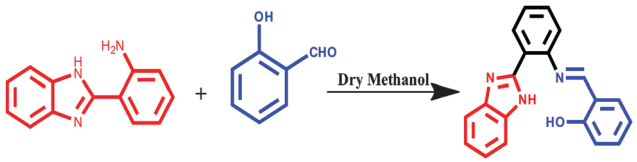

Scheme 1 Synthesis of **R1**.

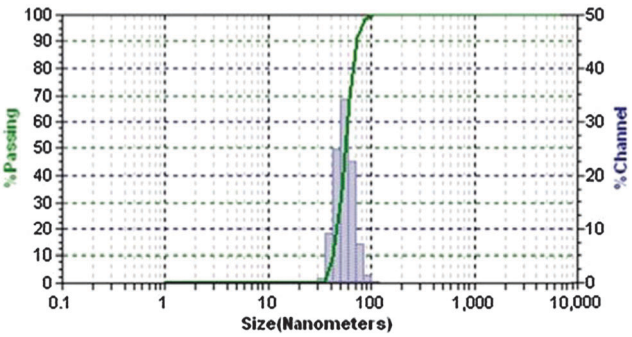

Fig. 1 Particle size distribution study of **N1** (showing an average particle size of 55 nm).

decoration of ZnO with **R1**, ZnO was synthesized *in situ* using dry ethanol using a method reported previously.[41] Dynamic light scattering (DLS) was employed for the analysis of the particle sizes of the **R1** decorated ZnO nanoparticles (Fig. 1).

It is quite evident from the DLS profile (Fig. 1) that the hydrodynamic diameter of **N1** is close to 55 nm. Decoration of the organic receptor on the ZnO particles is further validated using the EDX analysis data (shown in Fig. 2a). The presence of the carbon and nitrogen element peaks of the organic receptor

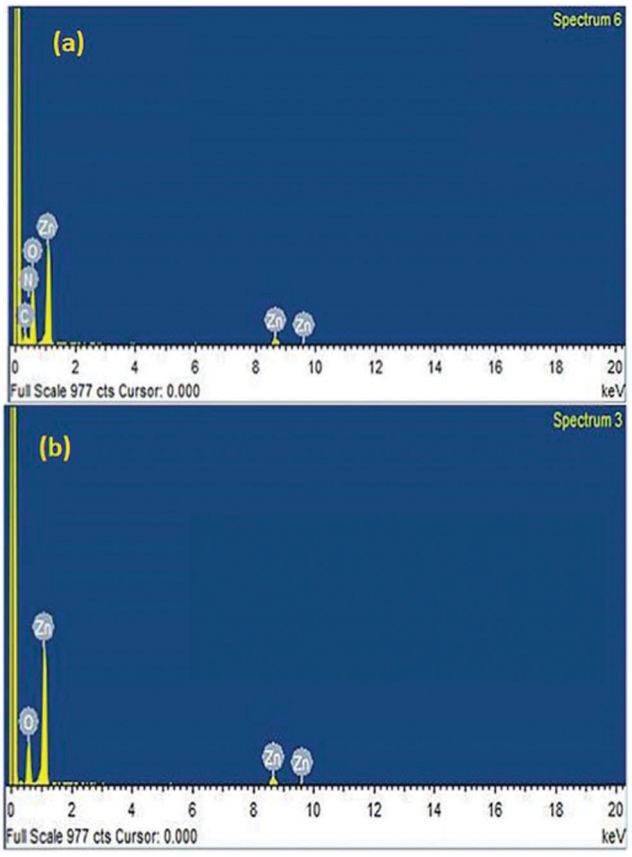

Fig. 2 (a) EDX analysis of **N1** confirming the presence of organic receptor (**R1**) on the ZnO particles (b) EDX analysis of **N1** after burning at 500 °C for 6 h (showing the removal of the organic receptor (**R1**) from the ZnO nanoparticles).

along with the oxygen and zinc element peaks confirms the decoration of **R1** on the ZnO nanoparticles. Thereafter, once the decorated samples were calcinated in a muffle furnace at 500 °C for 6 hours, the peaks of the organic receptor disappeared and peaks for only the Zn and O remained (shown in Fig. 2b).

Moreover, the morphology of compound **N1** can be predicted due to the non-covalent supramolecular interactions resulting in a self-assembled feather like structure (Fig. 3a). The particular growth of **N1** is probably expected due to the surface directing behaviour of **R1** which can control the shape and size of the ZnO particles. Various surface directing agents like surfactants, phospholipids, proteins, *etc.* have been used and are reported in the literature[43–45] to control the shape and size of metal oxide nanoparticles. To confirm the surface directing behaviour of **R1**, SEM images of **N1** (Fig. 3a) and **N1** after calcination (Fig. 3b) were recorded. It is quite evident from the scanning electron micrographs that the self-assembled feather like structures show the development of pores as the organic part is removed after calcination.

The calcinated product was further analysed using powder X-ray diffraction (Fig. 4). This further confirmed that only the pure ZnO crystals remained after calcination. The presence of a

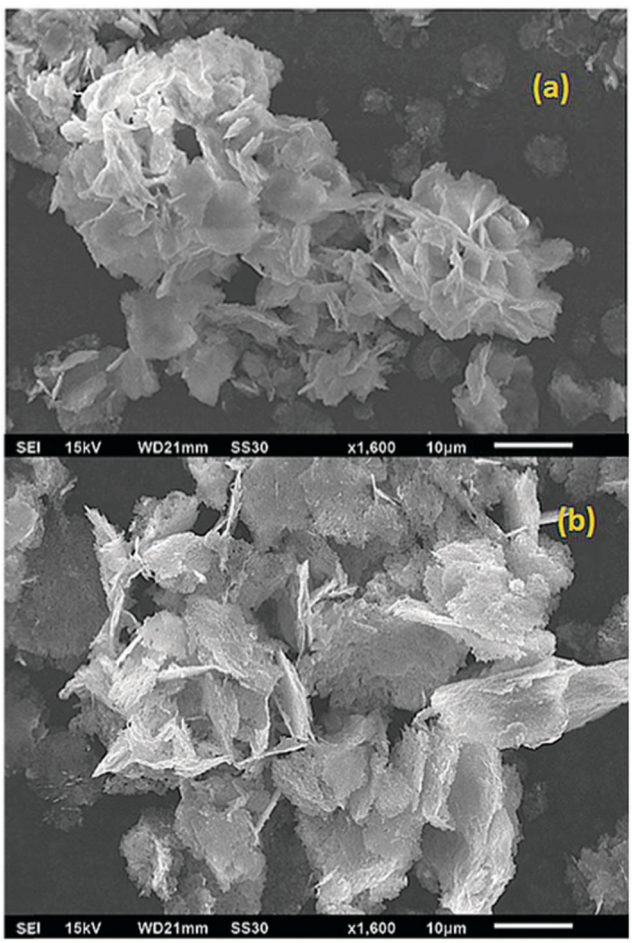

Fig. 3 Scanning electron micrographs of (a) compound **N1** and (b) **N1** after calcination.

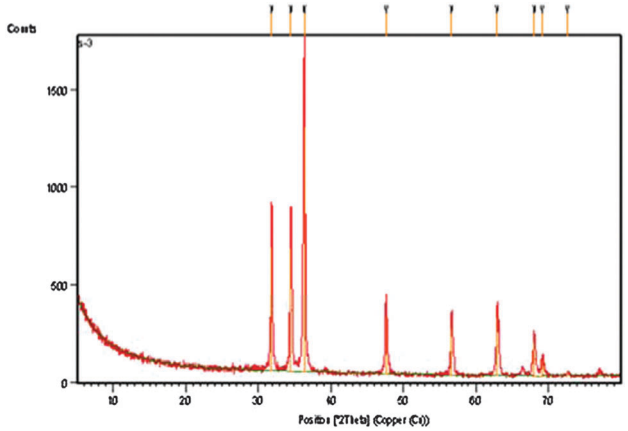

Fig. 4 XRD pattern of the ZnO nanoparticles (obtained by burning of **N1** at 500 °C for 6 h).

wurtzite structure has been indicated through the diffraction peaks at 31.8°, 34.4°, 36.3°, 47.6°, 56.6°, 62.9°, and 68.0°. These peaks correspond to the typical reflection planes of the wurtzite structure at (100), (002), (101), (102), (110), (103) and (112) of the ZnO nanoparticles.

No extra peaks other than those for ZnO are observed in the XRD data, which illustrated that **R1** has been completely burnt from the surface of the ZnO and only the ZnO is left behind. The Debye–Scherer equation has been employed for the calculation of the average crystallite size (D) of the ZnO nanoparticles.

$$D = 0.089\lambda/\beta\cos\theta$$

where, λ stands for the X-ray wavelength (0.154 nm), θ stands for the Bragg diffraction angle and β is the full width at half maximum (FWHM) of the diffraction peaks. The average crystallite size was calculated as ~35.16 nm. The small crystal size calculated from the XRD, authenticated the size estimated from the DLS, and confirmed the elimination of the organic receptors from the ZnO nanoparticles upon calcination of **N1**. To confirm the binding behaviour of the ZnO with **R1** to form **N1**, NMR and IR studies were performed. The NMR study showed the broadening of the peaks and the disappearance of the peak at 10.18 ppm (Fig. S3, ESI†) *i.e.* the peak of the phenolic proton due to the complexation with ZnO. Similarly, the Schiff's base peak at 1621 cm^{-1} (Fig. S4a, ESI†) had been shifted to 1615 cm^{-1} (Fig. S4b, ESI†) in the IR spectra. This shift in the peaks was also accompanied by a slight broadening of various peaks. It is quite evident from the results obtained that **R1** gets decorated on the surface of ZnO.

Metal binding studies

To determine the sensing ability of the **R1** decorated ZnO nanoparticles fluorescence spectroscopy was employed and a solution of **N1** was screened against several metal ions (K^+, Na^+, Ag^+, Pb^{2+}, Cu^{2+}, Cd^{2+}, Hg^{2+}, Fe^{2+}, Co^{2+}, Zn^{2+}, Ni^{2+} Fe^{3+}, Cr^{3+}, Mg^{2+} and Mn^{2+}) (Fig. 5).

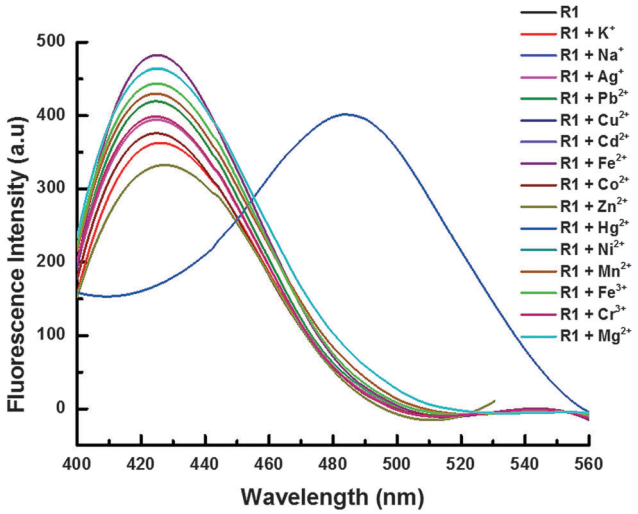

Fig. 5 Fluorescence intensity change of **N1** (10 nM) in the presence of 50 nM of metal nitrate solution in a HEPES buffered DMSO/water solvent system (70 : 30 v/v).

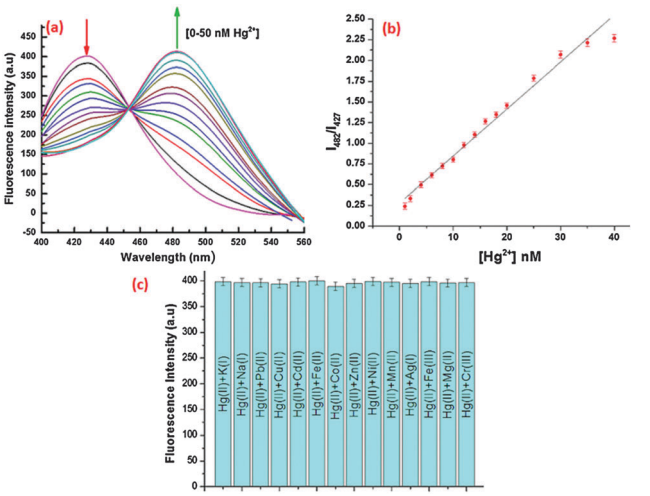

Fig. 6 (a) Fluorescence intensity change of **N1** (15 μM) upon the addition of small aliquots of mercury ions (0.5–50 nM) in a 7 : 3 ratio DMSO/water solvent system with a stabilized pH with HEPES buffer. (b) Calibration plot for Hg^{2+} ions plotting ratiometric fluorescence intensity *versus* the concentration of mercury ions added during the titration process. (c) Competitive binding studies of Hg^{2+}, when other metal ions are added as an interferent (Na^+, Pb^{2+}, K^+, Ag^+, Mn^{2+}, Zn^{2+}, Co^{2+}, Fe^{2+}, Cu^{2+}, Cd^{2+}, Fe^{3+}, Cr^{3+}, Mg^{2+} and Ni^{2+}) in a DMSO/water solvent system (7 : 3 v/v).

Addition of Hg^{2+} ions to the solution of **N1** resulted in a clear red shift in the fluorescence spectra of **N1** *i.e.* the fluorescence peak at 427 nm was gradually quenched on the addition of the Hg^{2+} ions and a new peak at 482 nm gradually emerged with the increased concentration of Hg^{2+} ions. While other metal ions (like K^+, Na^+, Ag^+, Pb^{2+}, Cu^{2+}, Fe^{2+}, Co^{2+}, Zn^{2+}, Ni^{2+}, Fe^{3+}, Cr^{3+}, Mg^{2+} and Mn^{2+}) showed no effect whatsoever on the emission profile of **N1** at 427 nm. From the above results it can be concluded that mercury ions can be determined selectively using **N1**. The selective binding of mercury ions with complex **N1** can be explained on the basis that ZnO has a great affinity to complex with the Schiff's base and hydroxyl ions of **R1**, leading to restricted rotation of **R1** around its axis. This restricted rotation provides the proper orientation and cavity to complex with various ions. Further selectivity for mercury can be attributed to the perfect fit cavity size of **N1** for the binding and encapsulation of mercury ions.

To further confirm the binding of **N1** with Hg^{2+} ions, a titration (Fig. 6a) was performed by adding small aliquots of Hg^{2+} ions (0–50 nM) into a solution of **N1** (10 nM) using a solvent mixture of DMSO/water (7 : 3, v/v); the fluorescence peak intensity at 427 nm slowly decreased and shifted towards the higher wavelength at 482 nm. The clear isosbestic point was achieved at 458 nm. The linear decrease in intensity at 427 nm and the gradual increase in the peak at 482 nm, with a clear isosbestic point, validates the use of **N1** for the ratiometric determination of Hg^{2+} ions in solutions of environmental and ecological importance. A calibration plot was made by plotting the ratiometric fluorescence intensity of **N1** *versus* the concentration of Hg^{2+} ions. It's quite evident from the calibration plot that **N1** responds linearly for Hg^{2+} ions up to 40 nM (Fig. 6b) with a regression coefficient of 0.9841. The proposed receptor has a minimum detection limit of 0.19 nM, calculated using the standard IUPAC 3σ method.[46]

It's been well documented in the literature that ratiometric estimation offers more accurate results compared with orthodox methods as it is less prone to errors like phototransformations, receptor concentration and environmental effects.[47] Furthermore, to explore the workability of a proposed sensor for real sample application, competitive experiments were performed with mixtures of Hg^{2+} as the primary ion and other metals (K^+, Na^+, Pb^{2+}, Cu^{2+}, Cd^{2+}, Fe^{2+}, Co^{2+}, Zn^{2+}, Ni^{2+}, Fe^{3+}, Cr^{3+}, Mg^{2+} and Mn^{2+}) as an interferent in a solution of **N1**. The emission profile of **N1** in the presence of Hg^{2+} ions showed no change upon the addition of various metal ion solutions added as interferents (Fig. 6c). From the above results it can be perceived that **N1** can be utilised as a sensor for the selective determination of mercury ions in samples of various analytical importance, without having any interference from other metal ions.

Real sample analysis

Real samples of mercury ions (H1–H4) were prepared by dissolving known concentrations of mercury ions. The samples thus obtained were analysed using the reported sensor and the results are reported in Table 1.

Table 1 Real sample analysis of mercury ions in artificially prepared samples made by dissolving known concentrations of mercury ions

S. no.	Sample	Conc. added (nM)	Conc. of mercury ions recovered[a] (nM)	Recovery (%)
1	H1	10	9.87 ± 0.03	98.7
2	H2	20	19.37 ± 0.07	96.85
3	H3	30	28.46 ± 0.04	94.87
4	H4	40	37.87 ± 0.04	94.68

[a] Mean of three determinations.

It is quite evident from Table 1 that **N1** can be used for the selective determination of Hg^{2+} ions in real samples of analytical importance, with an accuracy of more than 90%.

Conclusion

The organic receptor (**R1**) was synthesized and decorated on ZnO nanoparticles, and the compound formed (**N1**) was explored as a sensor for the selective determination of mercury ions in a semi-aqueous solvent system. The shape and size of the decorated ZnO nanoparticles were characterized using SEM, XRD and DLS studies. The binding affinity of the prepared sensor towards a library of metal ions such as K^+, Na^+, Ag^+, Pb^{2+}, Cu^{2+}, Cd^{2+}, Fe^{2+}, Co^{2+}, Zn^{2+}, Hg^{2+}, Ni^{2+}, Fe^{3+}, Cr^{3+}, Mg^{2+} and Mn^{2+} was performed in DMSO/water (7 : 3, v/v) and the ratiometric response upon the interaction with Hg^{2+} ions was recorded. Gradual addition of Hg^{2+} ions to a solution of **N1** quenched the fluorescence at 427 nm and an enhancement was observed at 482 nm, with a clear isosbestic point at 458 nm, having a lowest detection limit of 0.19 nM. Therefore, the ratiometric fluorescent sensor provides an alternate strategy of receptor coated ZnO nanoparticles for the nanomolar detection of Hg^{2+} ions.

Experimental section

Materials and methods

Commercial grade chemicals were purchased from Sigma-Aldrich; solvents of highest purity were purchased from SD fine chemicals and were used as received without any further purification. A JNMECS400 (JEOL) spectrophotometer has been used for recording the NMR spectra of **R1** and **N1**. A Shimadzu RF 5301-PC spectrofluorimeter has been employed for recording the emission profiles of **N1** and **R1**, while the UV-visible absorption spectra were recorded on a Shimadzu 2400 spectrophotometer with a quartz cell of path length 1 cm. A PANlytical X'PERT Pro diffractometer has been used for exploring the crystal structure of the ZnO powder samples. The diffractometer used Ni filtered Cu Kα radiation with a scan speed of 10° min^{-1} for 2θ in a range of 10–75. The data obtained was analysed using the Debye–Scherrer equation to get the crystal size. A scanning electron microscope (SEM-JEOL JSM 6610 LV) operating at a voltage of 15 kV has been employed for the morphology (SEM) and elemental analyses (EDX) of the **N1** and **N1** after calcination. The dynamic particle size of the **R1** decorated ZnO was measured using a Metrohm Microtrac Ultra Nanotrac particle size analyser (DLS). The whole study has been performed using a DMSO/water solvent system in the ratio of 7 : 3.

Synthesis of receptor 1 and decoration of the receptor on the ZnO nanoparticles

A single step condensation of 2-(2-aminophenyl)benzmidazole with salicylaldehyde has been employed for the preparation of receptor (**R1**) in dry methanol using a similar method as reported previously.[42] The prepared **R1** was characterized using IR, NMR and mass spectroscopy. The IR spectrum of **R1** was characterized with an imine linkage (–CH═N) peak at 1621 cm^{-1}. The ^1H NMR spectrum exhibited peaks at 6.62–6.68 (m, 1H, Ar), 6.80 (t, 1H, Ar), 6.86 (d, 1H, Ar), 6.90 (d, 1H, Ar), 7.09–7.24 (m, 6H, Ar), 7.27 (s, 1H, CH═N), 7.64 (d, 1H, Ar), 7.95 (d, 1H, Ar), and 10.18 (s, 1H, OH). ^{13}C NMR δ (ppm): 63.0, 110.2, 111.5, 114.8, 115.8, 117.8, 118.6, 119.3, 122.0, 122.2, 124.6, 126.1, 126.4, 130.0, 131.6, 132.9, 143.5, 143.8 and 147.3.

The ZnO nanoparticles were prepared by simultaneous mixing of $Zn(ClO_4)_2{\cdot}6H_2O$ and **R1** in dry ethanol under constant stirring at a temperature of 25 °C. Gradual addition of NaOH solution to the mixture of zinc perchlorate and **R1** led to the formation of a ZnO dispersion in the solution. The prepared dispersion was separated through centrifugation and washed 5 times with ethanol and water. The yielded product **N1** was dried at 50 °C for 24 h. SEM and EDX of the **N1** were recorded before and after calcination at 500 °C for 6 h in a muffle furnace.

Recognition properties of the receptor decorated ZnO (N1)

All the recognition studies were performed at ambient temperature. Prior to recording any spectra, sufficient time was provided after shaking the solutions to maintain its uniformity. Changes in the fluorescence profile of **N1** were used for analysing the cation binding affinity of **N1** toward different cations (K^+, Na^+, Ag^+, Pb^{2+}, Cu^{2+}, Cd^{2+}, Fe^{2+}, Co^{2+}, Zn^{2+}, Hg^{2+}, Ni^{2+}, Fe^{3+}, Cr^{3+}, Mg^{2+} and Mn^{2+}). The metal binding test of the **R1** decorated ZnO nanoparticles was performed by adding standard solutions of **N1** (10 nM) to a standard concentration of metal nitrate solution (50 nM) in a HEPES buffer stabilized DMSO : water solvent system with a ratio of 7 : 3. Similarly, for the titration experiment the gradual addition of mercury ions (0–50 nM) was made to a fixed concentration of **N1** (10 nM), with the same solvent system. The particle size distribution of the receptor decorated ZnO was measured using a probe based Metrohm microtrac Ultra nanotrac particle size analyzer. Interference studies were performed by adding various metal ions (K^+, Na^+, Ag^+, Pb^{2+}, Cu^{2+}, Cd^{2+}, Fe^{2+}, Co^{2+}, Zn^{2+}, Hg^{2+}, Ni^{2+}, Fe^{3+}, Cr^{3+}, Mg^{2+} and Mn^{2+}) as interferent ions along with the mercury ions as the primary ion in a DMSO : water solvent system in the ratio of 7 : 3 stabilized with a HEPES buffer.

Real sample analysis

A known concentration of mercury ions was dissolved to prepare various samples (H1–H4) and these were put under scrutiny using the reported sensor and the results thus obtained were compared in terms of percentage recovery.

Acknowledgements

This work has been supported by a Grant from CSIR, New Delhi through a research project sanctioned to Dr Navneet Kaur. Ms Narinder Kaur is thankful to Panjab University Chandigarh to allow her to work as summer trainee.

References

1 K. Tayade, S. K. Sahoo, S. Chopra, N. Singh, B. Bondhopadhyay, A. Basu, N. Patil, S. Attarde and A. Kuwar, *Inorg. Chim. Acta*, 2014, **421**, 538.
2 L. Y. Chen, C. M. Ou, W. Y. Chen, C. C. Huang and H. T. Chang, *ACS Appl. Mater. Interfaces*, 2013, **5**, 4383.
3 Y. Zhu, Y. Cai, Y. Zhu, L. Zheng, J. Ding, Y. Quan, L. Wang and B. Qi, *Biosens. Bioelectron.*, 2015, **69**, 174.
4 R. M. F. Batista, R. C. M. Ferreira, M. M. M. Raposo and S. P. G. Costa, *Tetrahedron*, 2012, **68**, 7322.
5 T. Raj, P. Saluja, N. Singh and D. O. Jang, *RSC Adv.*, 2014, **4**, 316.
6 Y. Weia, R. Yang, X. Chen, L. Wang, J. H. Liu and X. J. Huang, *Anal. Chim. Acta*, 2012, **755**, 54.
7 S. Wang, E. S. Forzani and N. Tao, *Anal. Chem.*, 2007, **79**, 4427.
8 K. Velmurugan and R. Nandhakumar, *J. Lumin.*, 2015, **162**, 8.
9 S. Chemate and N. Sekar, *Sens. Actuators, B*, 2015, **220**, 1196.
10 A. Singh, T. Raj, T. Aree and N. Singh, *Inorg. Chem.*, 2013, **52**, 13830.
11 K. Duarte, C. I. L. Justino, A. C. Freitas, A. M. P. Gomes, A. C. Duarte and T. A. P. R. Santos, *Trends Anal. Chem.*, 2015, **64**, 183.
12 M. Harada, Minamata disease: methylmercury poisoning in Japan caused by environmental pollution, *Crit. Rev. Toxicol.*, 1995, **25**, 1.
13 S. Pu, H. Jia, C. Fan, G. Liu, Y. Fu and S. Jing, *Tetrahedron*, 2015, **71**, 3463.
14 G. Hennrich, W. Walther, U. R. Genger and H. Sonnenschein, *Inorg. Chem.*, 2001, **40**, 641.
15 S. A. ElSafty, D. Prabhakaran, Y. Kiyozumi and F. Mizukami, *Adv. Funct. Mater.*, 2008, **18**, 1739.
16 E. M. Nolan and S. J. Lippard, *Chem. Rev.*, 2008, **108**, 3443.
17 H. H Harris, I. J. Pickering and G. N. George, *Science*, 2003, **301**, 1203.
18 A. Stacchiotti, F. Morandini, F. Bettoni, I. Schena, A. Lavazza, P. G. Grigolato, P. Apostoli, R. Rezzani and M. F. Aleo, *Toxicology*, 2009, **264**, 215.
19 G. V. Ramesh and T. P. Radhakrishnan, *ACS Appl. Mater. Interfaces*, 2011, **3**, 988.
20 V. Bhalla, R. Tejpal, M. Kumar and A. Sethi, *Inorg. Chem.*, 2009, **48**, 24.
21 M. Harnly, S. Seidel, P. Rojas, R. Fornes, P. Flessel, D. Smith, R. Kreutzer and L. Goldman, *Environ. Health Perspect.*, 1997, **105**, 424.
22 M. Legrand, C. J. Sousa Passos, D. Mergler and H. M. Chan, *Environ. Sci. Technol.*, 2005, **39**, 4594.
23 Y. A. Vilpan, I. L. Grinshtein, A. A. Akatove and S. Gucer, *J. Anal. Chem.*, 2005, **60**, 38.
24 J. M. Hightower and D. Moore, *Environ. Health Perspect.*, 2003, **111**, 604.
25 J. Chen, H. Chen, X. Jin and H. Chen, *Talanta*, 2009, **77**, 1381.
26 S. A. Malashikhin, K. K. Baldridge and N. S. Finney, *Org. Lett.*, 2010, **12**, 5.
27 S. Hussain, S. De and P. K. Iyer, *ACS Appl. Mater. Interfaces*, 2013, **5**, 2234.
28 Z. Zhu, Y. Su, J. Li, D. Li, J. Zhang, S. Song, Y. Zhao, G. Li and C. Fan, *Anal. Chem.*, 2009, **81**, 7660.
29 G. L. Wang, K. L. Liu, Y. M. Dong, Z. J. Li and C. Zhang, *Anal. Chim. Acta*, 2014, **827**, 34.
30 H. Goh, M. J. Kim, P. Saluja, N. Singh and D. O. Jang, *Tetrahedron Lett.*, 2012, **53**, 3900.
31 A. P. De Silva, T. S. Moody and G. D. Wright, *Analyst*, 2009, **134**, 2385.
32 L. B. Desmonts, D. N. Reinhoudt and M. C. Calama, *Chem. Soc. Rev.*, 2007, **36**, 993.
33 A. Asok, M. N. Gandhi and A. R. Kulkarni, *Nanoscale*, 2012, **4**, 4943.
34 U. Fegade, H. Sharma, N. Singh, S. Ingle, S. Attarde and A. Kuwar, *J. Lumin.*, 2014, **149**, 190.
35 K. Kaur, N. Kaur and N. Singh, *Mater. Lett.*, 2012, **80**, 78.
36 R. Li, Y. Luan, H. Zou, J. Du, T. Mud and Z. Li, *RSC Adv.*, 2012, **2**, 3049.
37 D. Barreca, D. Bekermann, E. Comini, A. Devi, R. A. Fischer, A. Gasparotto, C. Maccato, C. Sada, G. Sberveglieri and E. Tondello, *CrystEngComm*, 2010, **12**, 3419.
38 S. Kaur, A. Kaur and N. Kaur, *Mater. Lett.*, 2013, **100**, 19.
39 H. Sharma, N. Kaur, T. Pandiyan and N. Singh, *Sens. Actuators, B*, 2012, **166**, 467.
40 H. Sharma, K. Narang, N. Singh and N. Kaur, *Mater. Lett.*, 2012, **84**, 104.
41 H. Sharma, A. Singh, N. Kaur and N. Singh, *ACS Sustainable Chem. Eng.*, 2013, **1**, 1600.
42 P. Saluja, H. Sharma, N. Kaur, N. Singh and D. O. Jang, *Tetrahedron*, 2012, **68**, 2289.
43 P. Khullar, V. Singh, A. Mahal, P. N. Dave, S. Thakur, G. Kaur, J. Singh, S. S. Kamboj and M. S. Bakshi, *J. Phys. Chem. C*, 2012, **116**, 8834.
44 P. Khullar, A. Mahal, V. Singh, T. S. Banipal, G. Kaur and M. S. Bakshi, *Langmuir*, 2010, **26**, 11363.
45 M. S. Bakshi, S. Sachar, G. Kaur, P. Bhandari, G. Kaur, M. C. Biesinger, F. Possmayer and N. O. Petersen, *Cryst. Growth Des.*, 2008, **8**, 1713.
46 (*a*) G. L. Long and J. D. Wineforder, *Anal. Chem.*, 1980, **52**, 2242–2249; (*b*) A. Singh, A. Singh and N. Singh, *Dalton Trans.*, 2014, **43**, 16283–16288; (*c*) U. Fegade, S. K. Sahoo, A. Singh, P. Mahulikar, S. Attarde, N. Singh and A. Kuwar, *RSC Adv.*, 2014, **4**, 15288–15292.
47 H. J. Jung, N. Singh, D. Y. Lee and D. O. Jang, *Tetrahedron Lett.*, 2009, **50**, 5555.

